| | |
|---|---|
| Title | Oscillatory flow of a micropolar fluid as a model for blood flow |
| Sub Title | |
| Author | 澤田, 達男(Sawada, Tatsuo)<br>棚橋, 隆彦(Tanahashi, Takahiko)<br>安藤, 常世(Ando, Tsuneyo) |
| Publisher | 慶應義塾大学理工学部 |
| Publication year | 1982 |
| Jtitle | Keio Science and Technology Reports Vol.35, No.6 (1982. 7) ,p.105- 121 |
| JaLC DOI | |
| Abstract | The oscillatory flow of a micropolar fiuid in a circular tube is investigated, taking couple stress and spin angular momentum into consideration. The exact solutions for velocity, micro-rotation, vorticity, shearing stress, flow rate and energy dissipation are obtained mathematically. Further the energy dissipation over the cross section is calculated numerically. These solutions are characterized by three parameters, i.e. dimensionless frequency W which is called Womersley number, the ratio ε of vortex viscosity to shear viscosity, and the size effect parameter λ. The solutions are compared with those of Newtonian fluid and how to vary with ε and λ is discussed. Moreover the velocity profiles are compared with the experimental data observed in pulsatile blood flow by Bugliarello and Sevilla. |
| Notes | |
| Genre | Departmental Bulletin Paper |
| URL | https://koara.lib.keio.ac.jp/xoonips/modules/xoonips/detail.php?koara_id=KO50001004-00350006-0105 |

KEIO SCIENCE AND TECHNOLOGY REPORTS
VOL. 35, NO. 6, pp. 105-121, 1982

# OSCILLATORY FLOW OF A MICROPOLAR FLUID AS A MODEL FOR BLOOD FLOW

Tatsuo SAWADA*, Takahiko TANAHASHI** and Tsuneyo ANDO***

**Department of Mechanical Engineering, Keio University,
Hiyoshi, Yokohama 223, Japan**

*(Received, March 11, 1982)*

**ABSTRACT**

The oscillatory flow of a micropolar fiuid in a circular tube is investigated, taking couple stress and spin angular momentum into consideration. The exact solutions for velocity, micro-rotation, vorticity, shearing stress, flow rate and energy dissipation are obtained mathematically. Further the energy dissipation over the cross section is calculated numerically. These solutions are characterized by three parameters, i.e. dimensionless frequency $W$ which is called Womersley number, the ratio $\varepsilon$ of vortex viscosity to shear viscosity, and the size effect parameter $\lambda$. The solutions are compared with those of Newtonian fluid and how to vary with $\varepsilon$ and $\lambda$ is discussed. Moreover the velocity profiles are compared with the experimental data observed in pulsatile blood flow by Bugliarello and Sevilla.

## 1. Introduction

Classical continuum approach is based on the idea that all material bodies possess continuous mass densities, and that the constitutive equations are valid for every part of the body regardless of its size. In other words, a continuous mass density exists in a volume element that is infinitesimally small, and the symmetry of stress tensor can be assured. However, when fluids possess a substructure, e.g. polymers, blood, fluid suspensions, etc., the macroscopic limitation of the material volume element exists. Then the stress tensor is no longer symmetric, and there arises distributed couple per unit area across internal surfaces, i.e. couple stress.

For fluids which possess a substructure, there is another important loss of accuracy in classical continuum mechanics. When neutrally buoyant corpuscles are contained in fluid and velocity gradients in a flow field exist, corpuscles rotate, because of shearing stress. Hence, spin angular momentum is taken into account

* Graduate Student
** Associate Professor
*** Professor

in addition to the moment of linear momentum. (Spin angular momentum is also sometimes called intrinsic angular momentum.) Considering spin angular momentum, the symmetry of stress tensor is not assured, i.e. Cauchy's second law of motion for Newtonian fluids is no longer valid.

Fluid which has couple stress and spin angular momentum is called polar fluid or micropolar fluid. The theory of micropolar fluid was developed by Eringen (1968)[4] and Allen and DeSilva (1966)[1]. The behaviors of the fluid have been studied from various viewpoints. Stokes (1966, 1971)[9][10] discussed a few fundamental steady flows in order to determine material constants of the fluid which has couples stresses and also discussed some effects of couple stresses in fluids. But he did not take spin angular momentum into account. Shliomis (1967)[8] investigated hydrodynamics of a liquid with intrinsic rotation. Ramkissoon and Majumdar (1975)[6] considered a creeping flow past a sphere in micropolar fluids. They derived a simple formula for the drag in terms of the stream function. Ariman et al. (1974)[2] proposed a new spin boundary condition and investigated pulsatile flow of micropolar fluid by the method of Hankel transformation. They compared their theoretical results with the experimental data by Bugliarello and Sevilla (1970)[3] for both steady and pulsatile blood flows. Sawada and Tanahashi (1981)[7] analyzed a few basic flow patterns of micropolar fluid and discussed their apparent viscosities.

In this paper, we consider the oscillatory flow of micropolar fluid in a circular tube, using the theory advanced by Eringen. The flow behavior is investigated in detail for three important parameters. Analytical results are compared with those of Newtonian fluid which are obtained by Womersley (1955)[13] and Uchida (1956)[12]. Moreover the velocity profiles are compared with the analytical results of Ariman et al. and with the experimental data of Bugliarello and Sevilla observed in pulsatile blood flows.

## 2. Fundamental Equations

The equations which express the conservations of mass and linear momentum for micropolar fluids have the same form as they do for classical viscous fluids. Thus if we define the velocity vector $\boldsymbol{v}$, the stress tensor $\boldsymbol{T}$, the body force vector $\boldsymbol{b}$ and the density $\rho$ of the incompressible fluid which is considered here, the equations of continuity and momentum are expressed as follows:

$$\nabla\cdot\boldsymbol{v}=0, \tag{1}$$

$$\rho\frac{d\boldsymbol{v}}{dt}=\nabla\cdot\boldsymbol{T}+\rho\boldsymbol{b}. \tag{2}$$

The stress tensor is related to the velocity fields as in classical viscous fluid theory. For micropolar fluids, however, there is an additional contribution to the stress arising from the difference between micro-rotation $\boldsymbol{\Omega}$ and one-half of vorticity $\boldsymbol{\omega}$. If the stress tensor $\boldsymbol{T}$ is divided into two parts, i.e. the symmetric part $\boldsymbol{T}^s$ and antisymmetric part $\boldsymbol{T}^a$, the constitutive equations for the stress tensor are

$$\boldsymbol{T}^s=-p\boldsymbol{I}+\kappa(\mathrm{tr}\,\boldsymbol{D})\boldsymbol{I}+2\mu\boldsymbol{D}, \tag{3}$$

$$\boldsymbol{T}^a=-\mu_1\boldsymbol{I}\times(\boldsymbol{\omega}-2\boldsymbol{\Omega}), \tag{4}$$

where $p$ denotes the pressure, $\boldsymbol{D}$ is the rate of deformation tensor which represents the symmetric part of the velocity gradient, and $\boldsymbol{I}$ is the idemfactor. Further $\kappa$ is the second coefficient of viscosity, $\mu$ the shear viscosity and $\mu_1$ the vortex viscosity.

The second equation of Cauchy which expresses the conservation of angular momentum is

$$\frac{\rho\gamma}{\mu}\cdot\frac{d\boldsymbol{\Omega}}{dt}=\nabla\cdot\boldsymbol{M}+\rho\boldsymbol{l}+\boldsymbol{e}:\boldsymbol{T}^a,$$

where $\boldsymbol{M}$ is the couple stress tensor, $\boldsymbol{l}$ the body couple, $\gamma$ the material constant and $\boldsymbol{e}$ is the antisymmetric tensor of the third order. The constitutive equation of couple stress tensor $\boldsymbol{M}$ is as follows:

$$\boldsymbol{M}=\alpha\,\mathrm{tr}\,(\mathrm{grad}\,\boldsymbol{\Omega})\boldsymbol{I}+\beta\,\mathrm{grad}\,\boldsymbol{\Omega}+\gamma\,(\mathrm{grad}\,\boldsymbol{\Omega})^t, \tag{6}$$

where the material coefficients $\alpha,\beta$ and $\gamma$ have the dimension of momentum (namely, $[ML/T]$), which are called spin viscosity by Kline et al. (1972)[5].

Using Eq. (1), the substitution of Eqs. (3) and (4) into Eq. (2), and of Eq. (6) into Eq. (5) yields the following basic equations:

$$\rho\frac{d\boldsymbol{v}}{dt}=-\nabla p-(\mu+\mu_1)\nabla\times(\nabla\times\boldsymbol{v})+2\mu_1\nabla\times\boldsymbol{\Omega}+\rho\boldsymbol{b}, \tag{7}$$

$$\frac{\rho\gamma}{\mu}\cdot\frac{d\boldsymbol{\Omega}}{dt}=(\alpha+\beta+\gamma)\nabla\nabla\cdot\boldsymbol{\Omega}-\gamma\nabla\times(\nabla\times\boldsymbol{\Omega})+2\mu_1\nabla\times\boldsymbol{v}-4\mu_1\boldsymbol{\Omega}+\rho\boldsymbol{l}. \tag{8}$$

## 3. Oscillatory Flow in Circular Tube

Oscillatory flow of incompressible fluid in a rectilinear tube of circular section is considered here. It will be convenient to take the cylindrical coordinates whose $x$ axis is identified with the center line of the ture. We assume that neither body force nor body couple is present. We restric ourselves to the case

$$v_r=0,\quad v_\theta=0,\quad v_x=v(r,t), \tag{9}$$

$$\Omega_r=0,\quad \Omega_\theta=\Omega(r,t),\quad \Omega_x=0. \tag{10}$$

Here the equation of continuity (1) is automatically satisfied. On the restriction of Eqs. (9) and (10), Eqs. (7) and (8) are written as in cylindrical coordinates

$$(\mu+\mu_1)\frac{1}{r}\cdot\frac{\partial}{\partial r}\left(r\frac{\partial v}{\partial r}\right)+2\mu_1\frac{1}{r}\cdot\frac{\partial}{\partial r}(r\Omega)-\frac{\partial p}{\partial x}=\rho\frac{\partial v}{\partial t}, \tag{11}$$

$$\gamma\cdot\frac{\partial}{\partial r}\left\{\frac{1}{r}\cdot\frac{\partial}{\partial r}(r\Omega)\right\}-2\mu_1\frac{\partial v}{\partial r}-4\mu_1\Omega=\frac{\rho\gamma}{\mu}\cdot\frac{\partial\Omega}{\partial t}. \tag{12}$$

In the investigation of Ariman et al. the mathematical technique devised to obtain analytical solutions to the governing partial differential equations consists of application of consecutive transformations: a finite Hankel transform is made on the space variable (i.e. radial position, $r$) followed by a Laplace transform on time. This method is very complicated and calculation of the solutions cannot be performed easily. Then, we solve directly Eqs. (11) and (12) more easily.

The fundamental oscillating pressure gradient is expressed by

$$-\frac{\partial p}{\partial x}=A\exp(i\omega_0 t), \tag{13}$$

where $A$ is the amplitude of sinusoidal pressure gradient and $i$ is the imaginary unit. If $\omega_0 \to 0$, it gives the steady flow solution. The solutions of Eqs. (11) and (12) should be of the form

$$v(r,t)=\hat{v}(r)\exp(i\omega_0 t), \tag{14}$$

$$\Omega(r,t)=\hat{\Omega}(r)\exp(i\omega_0 t). \tag{15}$$

Only the real parts of these equations have the physical meaning. Substituting Eqs. (14) and (15) into Eqs. (11) and (12) leads simultaneous ordinary differential equations for $\hat{v}(r)$ and $\hat{\Omega}(r)$, that is,

$$(\mu+\mu_1)\frac{1}{r}\cdot\frac{d}{dr}\left(r\frac{d\hat{v}}{dr}\right)+2\mu_1\frac{1}{r}\cdot\frac{d}{dr}(r\hat{\Omega})-i\rho\omega_0\hat{v}=-A, \tag{16}$$

$$\gamma\frac{d}{dr}\left\{\frac{1}{r}\cdot\frac{d}{dr}(r\hat{\Omega})\right\}-2\mu_1\frac{d\hat{v}}{dr}-4\mu_1\hat{\Omega}=i\frac{\rho\omega_0\gamma}{\mu}\hat{\Omega}. \tag{17}$$

The general solutions for this system, which are finite at the tube axis $r=0$, are expressed by

$$\hat{v}(r)=-\frac{A}{m^2(\mu+\mu_1)}+\frac{2aC_1\mu_1}{(a^2+m^2)(\mu+\mu_1)}J_0(ar)+\frac{2bC_2\mu_1}{(a^2-b^2)(b^2+m^2)(\mu+\mu_1)}J_0(br), \tag{18}$$

$$\hat{\Omega}(r)=C_1J_1(ar)-\frac{C_2}{a^2-b^2}J_1(br), \tag{19}$$

where $C_1$ and $C_2$ are arbitrary integration constants. $a, b$ and $m$ are given by

$$\left.\begin{aligned} a^2&=-(4\mu\mu_1+i\rho\omega_0\gamma)/\gamma(\mu+\mu_1),\\ b^2&=-i\rho\omega_0/\mu,\\ m^2&=i\rho\omega_0/(\mu+\mu_1).\end{aligned}\right\} \tag{20}$$

The arbitrary integration constans $C_1$ and $C_2$ are determined by the boundary conditions on the wall of the tube. Though various arguments have been made for spin boundary conditions, a clear conclusion has not been obtained yet. The typical conditions are no-spin condition and constant-spin condition on the wall. The no-spin condition, which is suggested by Eringen, corresponds to the no-slip condition of velocity. This boundary condition is expressed by

$$v=0,\quad \Omega=0\quad \text{at}\quad r=R. \tag{21}$$

The analytical solutions under this condition were already reported in Ref. (11). The constant-spin condition is used by Ariman et al., which is based on the experimental results that corpuscles rotate on the wall. Here we use the constant-spin condition, which is written as

$$v=0, \frac{1}{r}\cdot\frac{\partial}{\partial r}(r\Omega)=0 \quad \text{at} \quad r=R. \tag{22}$$

Applying this condition to Eqs. (18), (19), (14) and (15) yields the desired solutions for $v$ and $\Omega$ as follows:

$$\bar{v}(\xi)=\frac{V(\xi)}{AR^2/4\mu}=-\frac{4}{\phi^2}\left[1-\frac{J_0(\delta)J_0(\phi\xi)+\frac{\phi^2\varepsilon}{\lambda^2(1+\varepsilon)}J_0(\phi)J_0(\delta\xi)}{\left\{1+\frac{\phi^2\varepsilon}{\lambda^2(1+\varepsilon)}\right\}J_0(\delta)J_0(\phi)}\right]\exp(i\omega_0 t), \tag{23}$$

$$\bar{\Omega}(\xi)=\frac{\Omega(\xi)}{AR/4\mu}=-\frac{2}{\phi}\cdot\frac{(\phi/\delta)J_0(\phi)J_1(\delta\xi)-J_0(\delta)J_1(\phi\xi)}{\left\{1+\frac{\phi^2\varepsilon}{\lambda^2(1+\varepsilon)}\right\}J_0(\delta)J_0(\phi)}\exp(i\omega_0 t), \tag{24}$$

where the bar means dimensionless quantity, and

$$\xi=r/R, \qquad \varepsilon=\mu_1/\mu,$$
$$W=R\sqrt{\rho\omega_0/\mu}, \qquad \phi=Wi^{3/2},$$
$$\lambda=R\sqrt{4\mu\mu_1/\gamma(\mu+\mu_1)}, \qquad \delta=\sqrt{\phi^2/(1+\varepsilon)-\lambda^2}.$$

These solutions are characterized by three dimensionless parameters $W$, $\lambda$ and $\varepsilon$, which are called Womersley number, the size effect parameter and the viscosity ratio, respectively.

Though both solutions of the authors and Ariman et al. are the same essentially, the representation of Eqs. (23) and (24) is much simpler than that obtained by Ariman et al. They slightly discussed about theoretical results of velocity and micro-rotation. Then we minutely investigate vorticity, shearing stress, flow rate and energy dissipation in addition to velocity and micro-rotation, and devote ourselves to get the clear influence of the dimensionless parameters.

### 3.1 Velocity Profiles

Velocity profiles at $\pi/8$ intervals during one half cycle are shown in Fig. 1. They are compared with velocity profiles of Newtonian fluid. When $W$ is large, the amplitude of the velocity decreases in proportion to $1/W^2$, which is verified by expanding Eq. (23) asymptotically. And the fluid flows with the phase lag of $\pi/2$ behind the pressure gradient. In the rapid oscillation it is found that the velocity profile becomes flat near the center of the cross section and the maximum velocity exists in the neighborhood of the wall, which is called the annular effect of oscillatory flow.

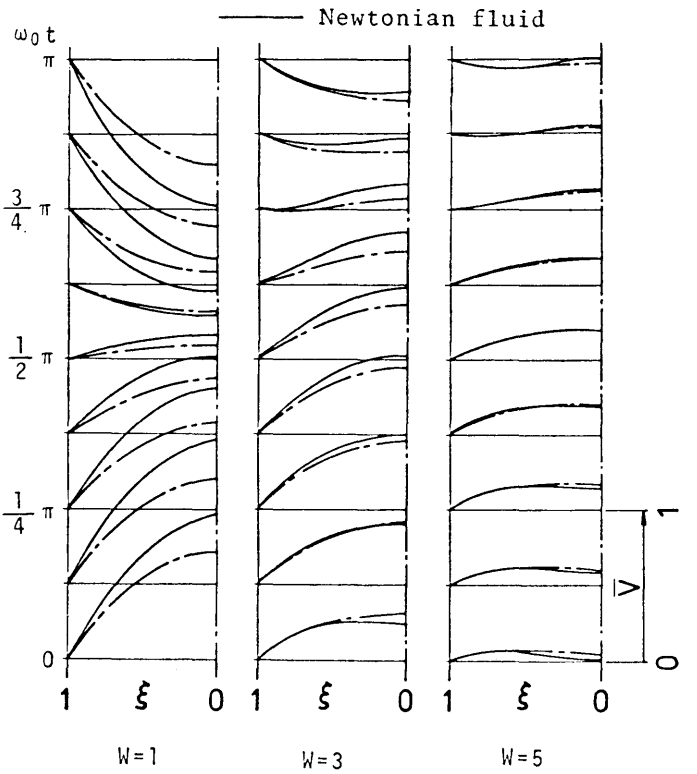


Fig. 1. Velocity profiles with $\lambda=1.0$ and $\varepsilon=1.0$

Figure 2 shows the variation of the velocity profiles for $\varepsilon$ and $\lambda$. As $\varepsilon$ becomes small, the velocity profile goes to that of Newtonian fluid. In general the micro-rotation of micropolar fluid is not equal to one-half of the vorticity which the velocity gradient produces. This difference yields the antisymmetric part of stress tensor. Vortex viscosity is a proportional constant in the antisymmetric part of stress tensor. $\varepsilon$ going to zero corresponds to the decrease of vortex viscosity. Then the antisymmetric part of stress tensor will be vanished in the limit. The micropolar effect does not appear in such a case.

While the parameter $\lambda$ indicates the size relation between corpuscle and tube radius. In the theory of micropolar fluid, it must be considered that corpuscles rotate because of shearing stresses. These rotations produce the micro-rotation,

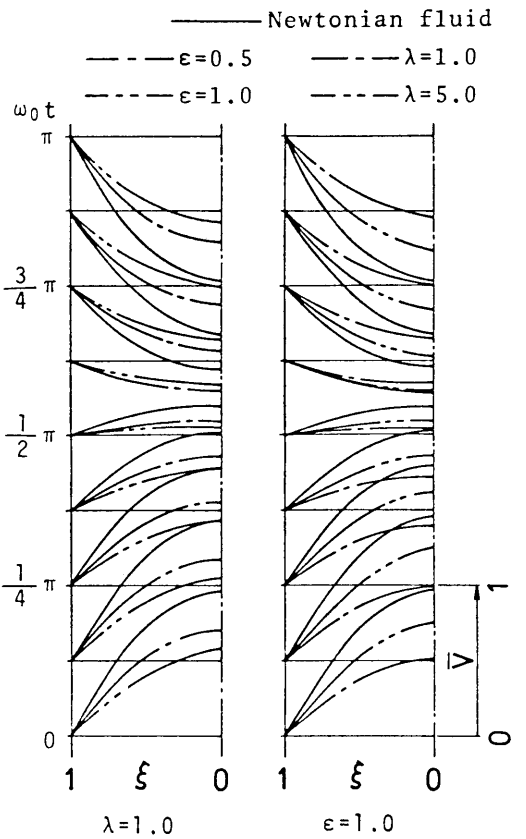


Fig. 2. Velocity profiles with $W=1.0$

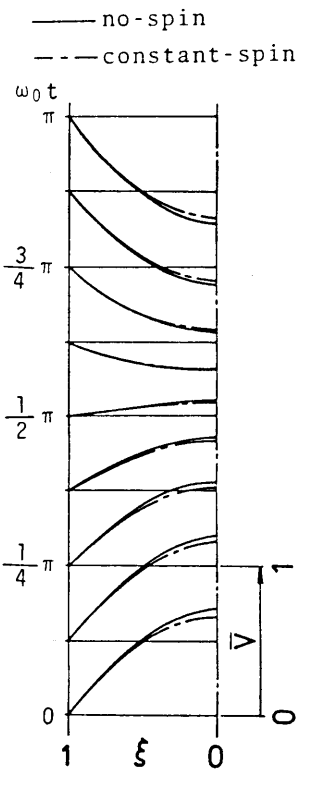


Fig. 3. Comparisons of velocity profiles between no-spin condition and constant-spin condition ($W=1.0, \lambda=1.0, \varepsilon=1.0$)

which has a relation with the volume averaged radius of gyration. If the radius of the circular tube changes, then the velocity profile varies. In Newtonian fluids the velocity profile does not depend on the tube radius. Now let $\lambda \to \infty$, i.e. the ratio of a tube radius to a corpuscle one be very large, then the velocity profile approaches that of Newtonian fluid.

Figure 3 shows the difference of velocity profiles between the constant-spin and no-spin conditions expressed by Eqs. (21) and (22), respectively. As may be seen from this figure, the velocity obtained by the no-spin condition is smaller than that obtained by the constant-spin condition near the center of the tube. Because the no-spin condition increases the resistance of the flow on the wall.

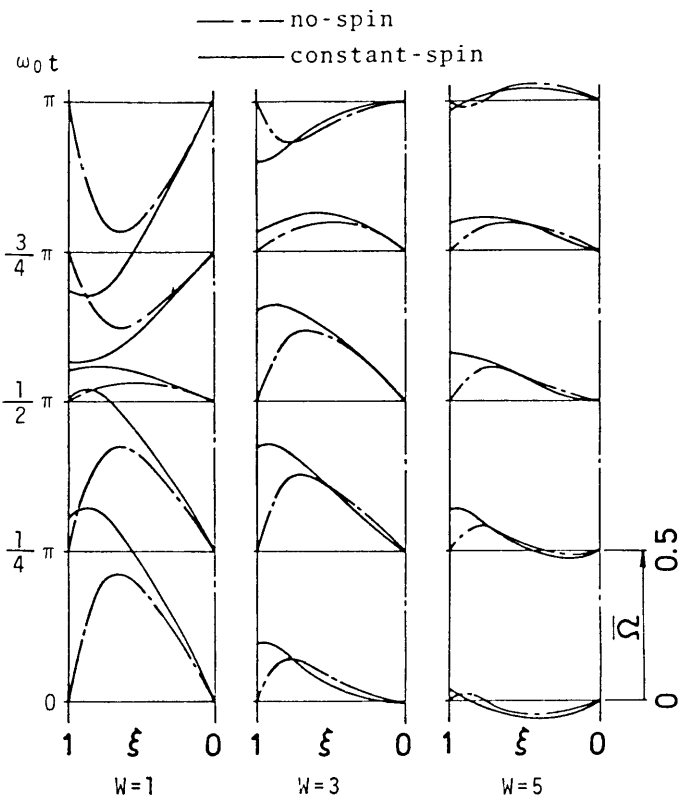


Fig. 4. Comparisons of micro-rotation between no-spin condition and constant-spin condition ($\lambda=5.0$, $\varepsilon=1.0$)

### 3.2 Micro-rotation and Vorticity

Distributions of micro-rotation at $\pi/4$ intervals over a half cycle are shown in Fig. 4. They are compared with those obtained by the no-spin condition. When $W$ increases, the amplitude of micro-rotation expressed by Eq. (24) diminishes in proportion to $1/W$ and $\Omega \to 0$ in the limit of $W \to \infty$. The variation of micro-rotation for $\varepsilon$ is no significant, but $\Omega$ is sensitive for $\lambda$ (see Fig. 5).

The vorticity vector $\boldsymbol{\omega}$ is defined as curl of the velocity vector. Then the nonzero component of vorticity vector is

$$\omega_\theta = -\frac{\partial v}{\partial r}. \tag{25}$$

Let us set $\omega=\omega_\theta$ for simplicity. Substituting Eq. (23) into Eq. (25) yields

$$\bar{\omega}(\xi)=\frac{\omega(\xi)}{AR/4\mu}=\frac{4}{\phi}\cdot\frac{J_0(\delta)J_1(\phi\xi)+\dfrac{\delta\phi\varepsilon}{\lambda^2(1+\varepsilon)}J_0(\phi)J_1(\delta\xi)}{\left\{1+\dfrac{\phi^2\varepsilon}{\lambda^2(1+\varepsilon)}\right\}J_0(\phi)J_0(\delta)}\cdot\exp(i\omega_0 t). \tag{26}$$

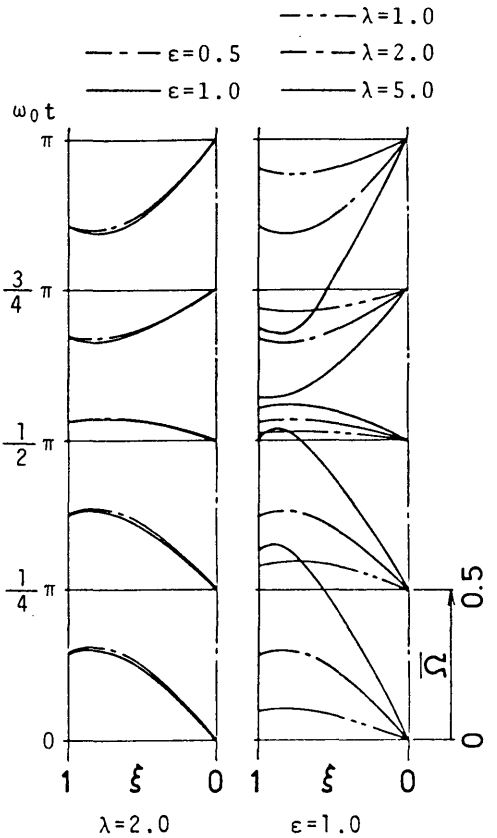


Fig. 5. Distributions of micro-rotation with $W=1.0$

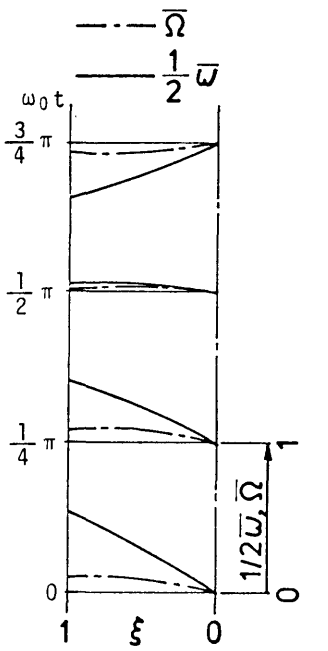


Fig. 6. Comparisons of distributions between micro-rotation and one-half of vorticity ($W=1.0$, $\lambda=1.0$, $\varepsilon=1.0$)

The antisymmetric part of stress tensor mainly consists of the difference of micro-rotation and one-half of vorticity. So comparison between them is shown in Fig. 6. When oscillation is extremely low, this difference becomes

$$\frac{\bar{\omega}}{2}-\bar{\Omega}=\frac{\phi}{\delta}\cdot\frac{\left\{1+\dfrac{\delta^2\varepsilon}{\lambda^2(1+\varepsilon)}\right\}J_1(\delta\xi)}{\left\{1+\dfrac{\phi^2\varepsilon}{\lambda^2(1+\varepsilon)}\right\}J_0(\delta)}\exp(i\omega_0 t)\rightarrow\frac{2}{\lambda(1+\varepsilon)}\cdot\frac{I_1(\lambda\xi)}{I_0(\lambda)}. \tag{27}$$

Then micro-rotation is smaller than one-half of vorticity in the case of $W\rightarrow 0$.

### 3.3 Shearing Stress

The component of shearing stress $T_{rx}$ will be obtained as follows:

$$T_{rx}=(\mu+\mu_1)\frac{\partial v}{\partial r}+2\mu_1\Omega. \tag{28}$$

Let us set $\tau=T_{rx}$. Substituting Eqs. (23) and (24) into Eq. (28) leads to

$$\bar{\tau}(\xi)=\frac{\tau(\xi)}{AR/2}=-\frac{2}{\phi}\cdot\frac{J_0(\delta)J_1(\phi\xi)+\dfrac{\phi\varepsilon}{\delta}\left(1+\dfrac{\delta^2}{\lambda^2}\right)J_0(\phi)J_1(\delta\xi)}{\left\{1+\dfrac{\phi^2\varepsilon}{\lambda^2(1+\varepsilon)}\right\}J_0(\phi)J_0(\delta)}\exp(i\omega_0 t). \tag{29}$$

Figure 7 shows the distributions of shearing stress. The dimensionless wall shearing stress is given by

$$\bar{\tau}_w=\left[-\frac{1+\varepsilon}{2}\bar{\omega}+\varepsilon\bar{\Omega}\right]_{\xi=1}. \tag{30}$$

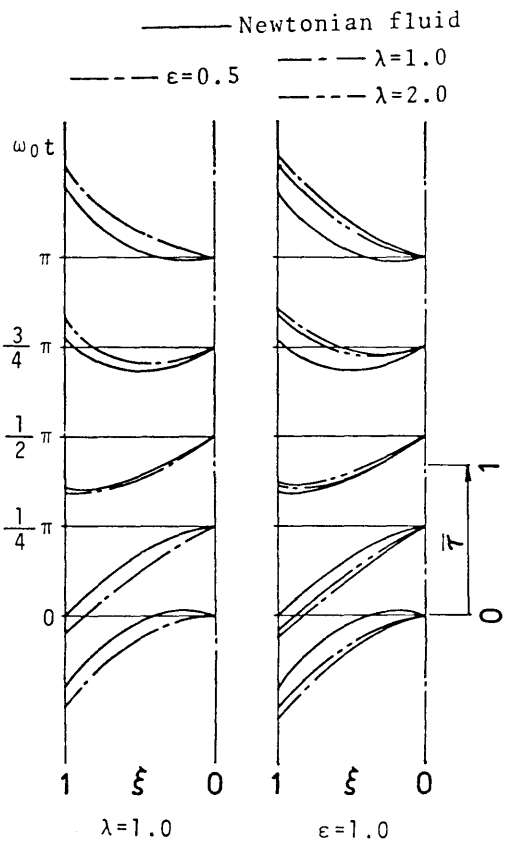


Fig. 7. Distributions of shearing stress with $W=3.0$

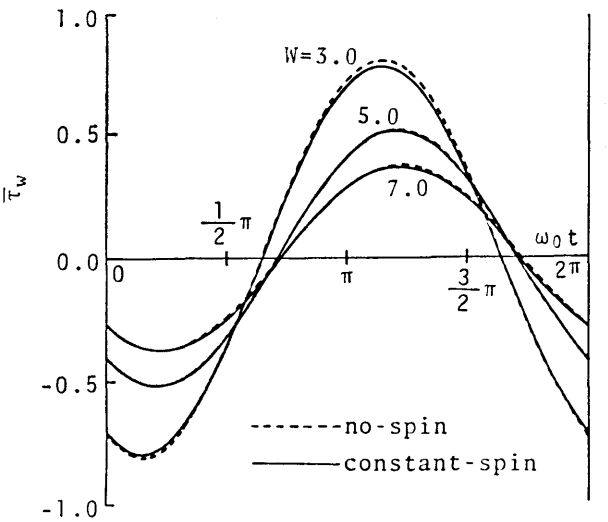


Fig. 8. Comparisons of wall shearing stress between no-spin condition and constant-spin condition ($\lambda=1.0$, $\varepsilon=1.0$)

The wall shearing stress in the no-spin condition is expressed only by the vorticity because $\bar{\Omega}(\xi=1)=0$. But the micro-rotation in the constant-spin condition is necessary in addition to the vorticity. In Fig. 8, the variations of the wall shearing stress for $W$ are shown over one cycle. If the boundary conditions are different on the wall, it may be expected that some change occurs in the wall shearing stress. But we observe a slight variation between the wall shearing stresses obtained by the two boundary conditions. The reason is considered to be the fact that the micro-rotation $\Omega$ offsets the increase of the vorticity on the wall.

### 3.4 Flow Rate

The volume flow rate is given by

$$Q(t)=\int_0^R 2\pi r v(r)dr. \tag{31}$$

Hence the dimensionless flow rate is defined by

$$\bar{Q}(t)=\frac{Q(t)}{\pi AR^4/8\mu}=-\frac{8}{\phi^2}\left[1-\frac{(2/\phi)J_0(\delta)J_1(\phi)+\dfrac{2\phi^2\varepsilon}{\delta\lambda^2(1+\varepsilon)}J_1(\delta)J_0(\phi)}{\left\{1+\dfrac{\delta^2\varepsilon}{\lambda^2(1+\varepsilon)}\right\}J_0(\delta)J_0(\phi)}\right]\exp(i\omega_0 t). \tag{32}$$

Variations of the flow rate with $\lambda$ and $\varepsilon$ are shown in Figs. 9 and 10. Curves representing the flow rate is similar to those of the volocity. The influence of $\lambda$ and $\varepsilon$ on $Q$ is quite analogous to that on the velocity profile.

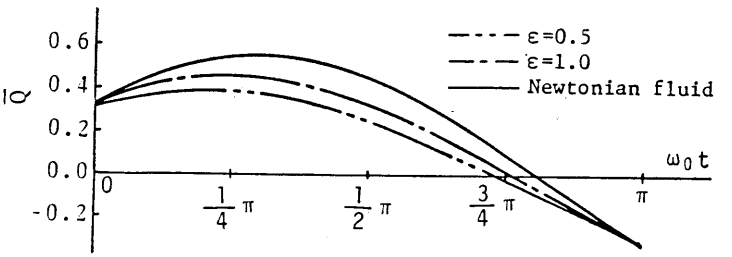


Fig. 9. Variations of flow rate with $\varepsilon$ ($W$=3.0, $\lambda$=1.0)

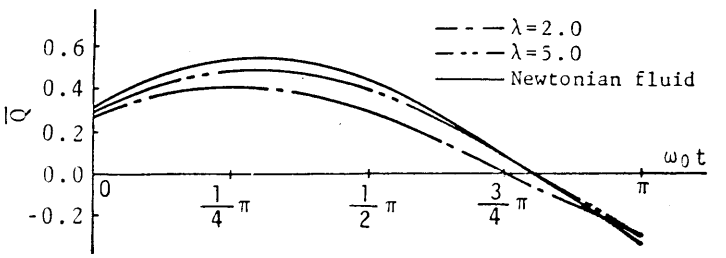


Fig. 10. Variations of flow rate with $\lambda$ ($W$=3.0, $\varepsilon$=1.0)

### 3.5 Energy Dissipation

The dissipation of energy per unit volume due to internal friction is given by the dissipation function

$$\Phi=\boldsymbol{T}^a:\boldsymbol{D}+\boldsymbol{M}:\nabla\boldsymbol{\Omega}+\left(\frac{1}{2}\boldsymbol{\omega}-\boldsymbol{\Omega}\right)\cdot\boldsymbol{e}:\boldsymbol{T}^a. \tag{33}$$

In cylindrical coordinates this function is written by

$$\Phi=\mu\left(\frac{\partial v}{\partial r}\right)^2+4\mu_1\left(\frac{1}{2}\cdot\frac{\partial v}{\partial r}+\Omega\right)^2-2\beta\left(\frac{\Omega}{r}\cdot\frac{\partial v}{\partial r}\right)+\gamma\left\{\left(\frac{\Omega}{r}\right)^2+\left(\frac{\partial\Omega}{\partial r}\right)^2\right\}. \tag{34}$$

Both the third and forth terms of the right-hand side of this equation can be neglected since their effects are small in comparison with the first and second terms. Substituting the solutions of the velocity and the micro-rotation into Eq. (34), we obtain

$$\Phi(\xi)=\frac{\Phi(\xi)}{A^2R^2/4\mu}=4\left[Re\left\{-\frac{1}{\phi}\cdot\frac{J_0(\delta)J_1(\phi\xi)+\dfrac{\delta\phi\varepsilon}{\lambda^2(1+\varepsilon)}J_0(\phi)J_1(\delta\xi)}{\left\{1+\dfrac{\phi^2\varepsilon}{\lambda^2(1+\varepsilon)}\right\}J_0(\delta)J_0(\phi)}\exp(i\omega_0 t)\right\}\right]^2$$

$$+4\varepsilon\left[Re\left\{\frac{1}{2\delta}\cdot\frac{\left\{1+\dfrac{\delta^2\varepsilon}{\lambda^2(1+\varepsilon)}\right\}J_1(\delta\xi)}{\left\{1+\dfrac{\phi^2\varepsilon}{\lambda^2(1+\varepsilon)}\right\}J_0(\delta)}\exp(i\omega_0 t)\right\}\right]^2. \tag{35}$$

When Womersley number $W$ is not large, the maximum of energy dissipations occurs on the wall of the tube. In the rapid oscillation, the maximum of energy dissipations takes place at a location slightly inside the wall, depending on the phase as shown in Figs. 11 and 12. The energy dissipations over the cross section are plotted in Fig. 13. The analytical expression for energy dissipation over the cross section cannot be explicitly obtained because of difficulty of the intergration of Bessel functions. These curves are calculated numerically by means of Simpson's rule. Here the dimensionless form is expressed as follows:

$$\overline{\int_0^R \Phi \cdot 2\pi r dr} = \int_0^R \Phi \cdot 2\pi r dr \Big/ \frac{\pi R^4 A^2}{8\mu}.$$

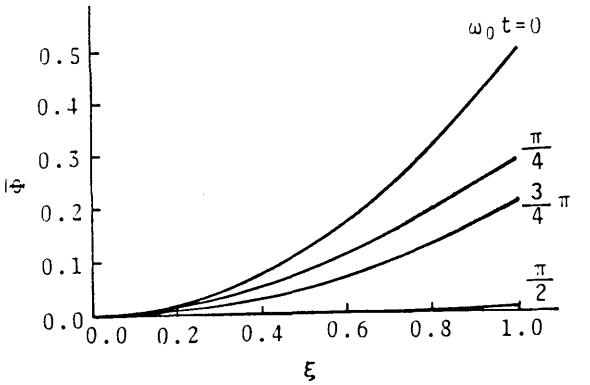


Fig. 11. Distributions of enery dissipation ($W=1.0$, $\lambda=1.0$, $\varepsilon=1.0$)

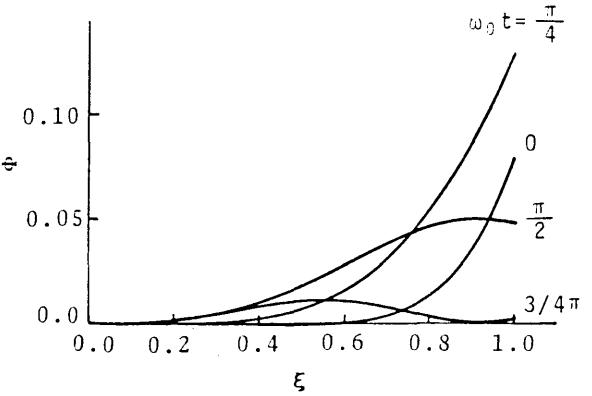


Fig. 12. Distributions of energy dissipation ($W=1.0$, $\lambda=1.0$, $\varepsilon=1.0$)

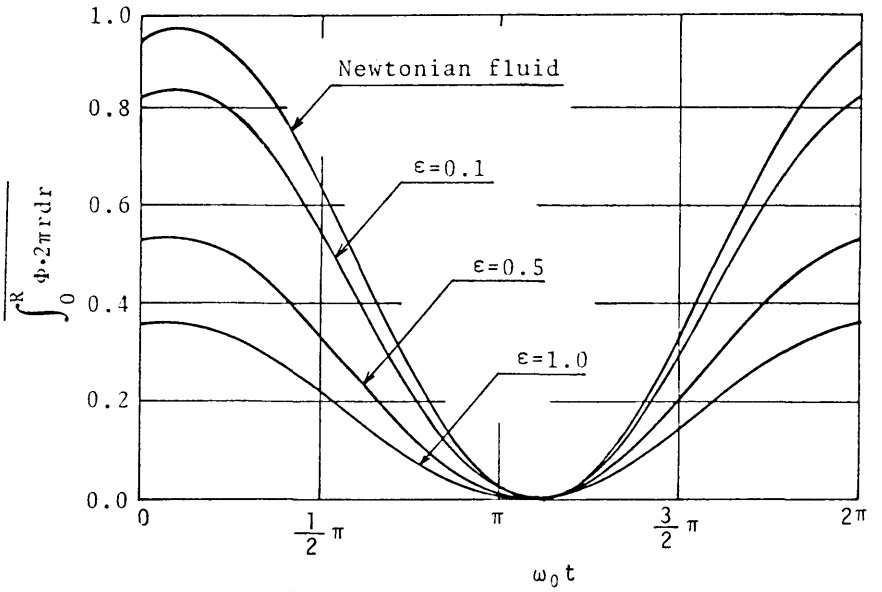


Fig. 13. Variations of energy dissipations overy the cross section ($W=1.0$, $\lambda=1.0$)

## 4. Comparison with theoretical and experimental results

Bugliarello and Sevilla (1970) made high-speed microcinematographical measurements of velocity profiles for steady and pulsatile flows of human blood in glass tubes, between 40 and 70 $\mu$m in nominal diameter. Now we shall compare the theoretical results with the experimental data obtained by Bugliarello and Sevilla using blood flow. In their experiment the frequency is 8.4 Hz and the oscillating component of the pressure wave has a half amplitude of the average pressure. The theoretical pulsatile velocity is obtained by superposing the velocity of steady flow on Eq. (23). The steady velocity is given by as follows:

$$\bar{v}(\xi)=1-\xi^2+\frac{4\varepsilon}{\lambda^2(1+\varepsilon)}\cdot\frac{I_0(\lambda\xi)-I_0(\lambda)}{I_0(\lambda)}. \tag{36}$$

To accomplish the comparison, it is necessary to determine the values of the material constants $\mu$, $\mu_1$ and $\gamma$ as functions of hematocrit. Since Ariman et al. (1974) compared their theoretical analysis with experimental results of Bugliarello and Sevilla, we use the same values used by Ariman et al. These material constants and dimensionless parameters used in the calculation are shown in Table 1.

Table 1 Material constants and dimensionless parameters

| $H$ % | $R$ $\mu$m | $\mu$ mPa·s | $\mu_1$ mPa·s | $\gamma$ kg·m/s | $W$ | $\varepsilon$ | $\lambda$ |
|---|---|---|---|---|---|---|---|
| 10 | 20 | 1.2 | 0.78 | $3.2\times10^{-13}$ | 0.14 | 0.65 | 1.5 |
| 20 | 20 | 1.2 | 0.92 | $5.8\times10^{-13}$ | 0.14 | 0.77 | 1.2 |
| 40 | 20 | 1.2 | 0.98 | $1.2\times10^{-12}$ | 0.14 | 0.82 | 0.85 |

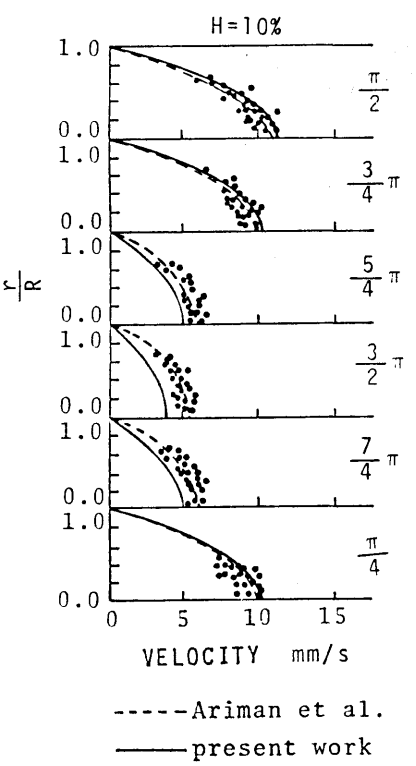


Fig. 14. Comparisons of theoretical velocity profiles with experimental pulsatile blood flow data of Bugliarello and Sevilla

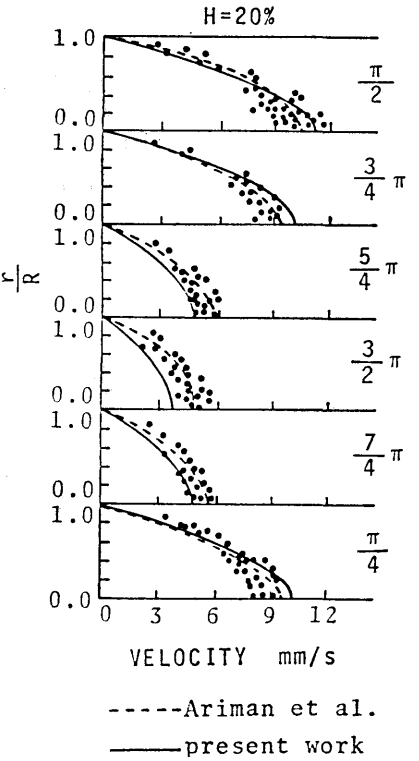


Fig. 15. Comparisons of theoretical velocity profiles with the experimental pulsatile blood flow data of Bugliarello and Sevilla

In Figs. 14, 15 and 16, the experimental velocity profiles measured in the 40 $\mu$m tube at 6 points in the pressure cycle are shown for three hematocrits.

From Figs. 14, 15 and 16, we have a favorable agreement between the theoretical results and the experimental pulsatile blood flow data of Bugliarello and Sevilla. But as for the amplitude, our results are a little larger than the results of Ariman et al. and the experimental data. Because the ambiguity of the data for pressure gradients may be considered to make a little error.

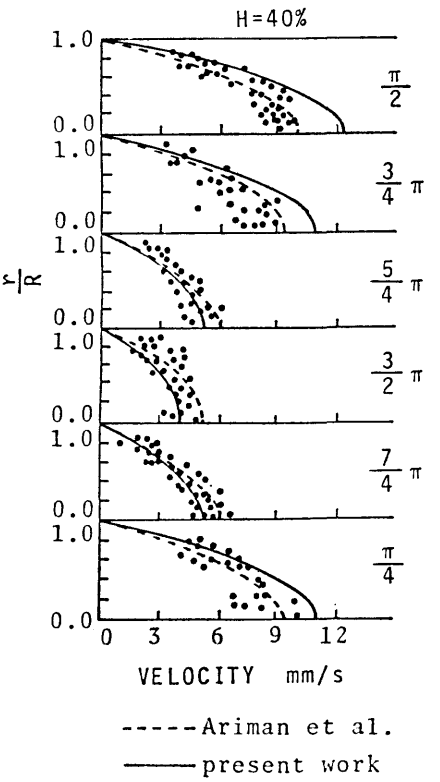


Fig. 16. Comparisons of theoretical velocity profiles with the experimental pulsatile blood flow data of Bugliarello and Sevilla

## 5. Conclusions

In this present paper, the oscillatory flow of a micropolar fluid has been studied mathematically on the basis of the theory advanced by Eringen. Exact solutions of the first and second Cauchy's equations, i.e. velocity, micro-rotation, vorticity, shearing stress, flow rate and energy dissipation, are obtained. They are characterized by three parameters, i.e. the dimensionless frequency $W$ (Womersley number), the size effect parameter $\lambda$ and the viscosity ratio $\varepsilon$. The latter two parameters present the characteristics of micropolar fluid. For high frequencies, the amplitude of velocity is inversely in proportion to the second power of Womersley number, while that of micro-rotation is inversely in proportion to the first power of Womersley number. For low frequencies, the flow of fluid becomes quasi-steady. The phase lag of velocity behind pressure diminishes gradually. A large value of size effect parameter makes the micropolar fluid approach the Newtonian behavior, then micro-rotation becomes equal to one-half of vorticity. When the ratio of viscosities becomes small, the polarity of fluid diminishes and micro-rotation reduces to zero. The difference of the boundary conditions adopted here causes the follow-

ing conclusions: in the no-spin condition the wall shearing stress is given by only the vorticity whereas in the constant-spin condition by the micro-rotation in addition to the vorticity, but this difference hardly influences the wall shearing stress; the velocity obtained from the no-spin condition is smaller than that obtained from the constant-spin condition. The comparison with the theoretical resuluts and the experimental pulsatile blood flow of Bngliarello and Sevilla seems to have a good agreement.

**Acknowledgements**

The authors wish to acknowledge that editing and typing of the manuscript were made with the aid of the word-processor of HITAC M-280 H of Tokyo University Computer Center. This work has been partly supported by Grant-in-Aid for Scientific Research from the Ministry of Education, Science and Culture, of Japan.

**REFERENCES**

[1] Allen, S.J. and DeSilva, C.N., J. Fluid Mech., Vol. 24, part 4 (1966), pp. 801-821.
[2] Ariman, T., et al., Trans. ASME, J. Appl. Mech., Vol. 41, No. 1 (1974), pp. 1-7.
[3] Bugliarello, G. and Sevilla, J., Biorheology, Vol. 7, No. 2 (1970), pp. 85-95.
[4] Eringen, A.C., Int. J. Eng. Sci., Vol. 2, No. 2 (1964), pp. 205-217.
[5] Kline, K.A., et al., Biorheology, Vol. 9, No. 1 (1972), pp. 1-22.
[6] Ramkissoon, H. and Majumdar, S.R., Letters Appl. Eng. Sci. Vol. 3 (1975), pp. 113-142.
[7] Sawawada, T. and Tanahashi, T., Bull. JSME, Vol. 24, No. 196 (1981), pp. 1778-1786.
[8] Shliomis, M.I., Sov. Phys. JETP, Vol. 124, No. 1 (1967), pp. 173-177.
[9] Stokes, V.K., Phys. Fluids, Vol. 9, No. 9 (1966), pp. 1709-1715.
[10] Stokes, V.K., Phys. Fluids, Vol. 14, No. 7 (1971), pp. 1580-1582.
[11] Tanahashi, T., et al., Trans. Jpn. Soc. Mech. Eng., Ser. B, Vol. 45, No. 389 (1979), pp. 20-27.
[12] Uchida, S., Z. Angew. Math. Phys., Vol. 7, No. 5 (1956), pp. 403-422.
[13] Womersley, J.R., Phil. Mag., Vol. 46, No. 373 (1955), pp. 199-221.